RESEARCH ARTICLE

VOLCANICA

Relating glassy rind thicknesses to ambient air temperatures at the Lost Jim flow field in the Imuruk Lake volcanic field, Alaska: A preliminary report

Erika Rader*[α], Jessica Larsen[β], Tim Orr[γ], Dawn Ruth[δ], and Jessica Stanley[α]

[α]Earth and Spatial Sciences, University of Idaho, ID, USA.
[β]Geophysical Institute and Department of Geosciences, University of Alaska Fairbanks, AK, USA.
[γ]U.S. Geological Survey, Anchorage, AK, USA.
[δ]U.S. Geological Survey, Moutain View, CA, USA.

Submitted: 2025-06-05 | Accepted: 2026-05-07 | Published: 2026-05-18

Editor: A. Whittington | Production: B. Hosseini; E.C. Hughes

Abstract

The Lost Jim flow field, in the Imuruk Lake volcanic field, Alaska, extends west ~34 km from a single vent, crossing subarctic tundra and currently touches several lakes and streams. The weighted mean of five ^{36}Cl cosmogenic exposure ages from the Lost Jim pāhoehoe flow is 7.73 ± 0.37 ka, indicating this eruption occurred substantially after the eruption of the underlying Camille flow, which was emplaced at 39.7 ± 1.3 ka. Paleoclimate records indicate the period when the Lost Jim flow field was emplaced was after deglaciation, and the climate was similar to today. We propose that the emplacement of lava in these cold subarctic conditions can lead to faster cooling of the lava surface compared to lava emplaced in warmer locations such as mid-latitude cold deserts. Glass abundance in the outermost rinds at the Lost Jim flow field was on average 74 % with 6.4 mm thick rims, compared to 60 % with 2.9 mm rims for cold mid-latitude desert samples. We interpret increased glass content as a proxy for rapid cooling likely occurring partly during winter. Glassiness values varied less across vent, margin, and mid-flow locations when compared to the mid-latitude flows suggesting the Lost Jim flow field was broadly impacted by the subarctic climate as opposed to responding to local microclimates. Our results indicate that lava glassiness may be a useful environmental indicator of cooler (in this case subarctic) conditions.

Keywords: Climate proxy; Vitric rind; Lava cooling rate; Pahoehoe; Mars.

1 Introduction

The outermost portion of a cooling lava flow will experience, and respond to, the conditions of the environment in which it is emplaced. If this response is substantial, reliable, and repeatable, then it would be possible to infer environmental factors at the time of emplacement from the state of the rind of an old lava flow. The scientific literature supports a substantial and reliable impact of glassy rind formation in sub-aqueous lava flows, but little has been done to explore the variety of cooling environments that may influence rind formation on lava flows. We present an evaluation of rind qualities from a subarctic lava flow which suggests that further investigation into lava cooling processes could be fruitful for studying past weather and climate conditions.

1.1 Lava cooling mechanisms

Lava flow surfaces are cooled via radiative heat loss and convective cooling as fluids (air or water on Earth) move across the surface [Head and Wilson 1986; Keszthelyi and Denlinger 1996; Griffiths 2000]. Radiative cooling dominates the initial drop in temperature as the heat loss is exponentially large when the lava is the hottest [Head and Wilson 1986]. Given that the only variable in radiative cooling between two lava flows on the same planet is the difference in their starting temperature, the impact of this component of heat loss is likely to be very similar between environments. However, cooling by convection can be heavily influenced by the surrounding environment—notably, exposure to wind and water can greatly increase the cooling rate of flow surfaces by changing h, the convective heating coefficient [Harris and Rowland 2001; Keszthelyi et al. 2003]. Even the presence of snow and ice in contact with any side of the flow (under, on top, or beside) can cool the top of a lava flow faster, either by direct contact with meltwater dripping onto the flow or steam plumes blowing against the surface from margin contact [Edwards et al. 2014; 2015]. However, interaction with snow or ice is likely to lead to distinctive cooling joint systems in the lavas and should be readily recognisable [Mee et al. 2006; Edwards et al. 2014; 2015]. One environmental factor that impacts convective cooling rate is the ambient atmospheric temperature; yet, this is less studied, as the change is smaller and, on the scale of cooling an entire flow field, the impact is small [Hirashima 1952; Patrick et al. 2004]. However, decreasing the ambient air temperature does increase heat flux, having an effect that would be most concentrated on the outermost surface of the flow. Thus, in a setting where two identical lava flows were cooling in different thermal environments, the outer rind of the lava flow in the colder environment would experience a faster cooling rate [Rowland et al. 2004]. Sufficient studies to assess the magnitude of this impact on glass formation have not been conducted; however, if we assume that small changes in cooling rate can influence the outermost surface of a flow, then these external environmental factors, including ambient

* erader@uidaho.edu

temperature, may be responsible for differences in surface rim characteristics.

1.2 Glassiness related to emplacement environment

The impact of faster cooling and rind formation has not yet been studied at various air temperatures, but a more extreme example—lava-water interactions—can be useful for considering the outcome of colder ambient temperatures. The connection between water-influenced emplacement and lava glassiness is well established, with increased cooling rates leading to thicker glassy rinds [Keszthelyi and Denlinger 1996]. Lava that interacts with abundant water, such as in undersea eruptions, develops a rind several cm thick [Wilding et al. 1995; 1996; 2000; Nichols et al. 2009]. Flows that encounter water sources even minimally will develop a visibly glassy rind that is 25 % thicker than air-cooled lavas [Lescinsky and Fink 2000; Deschamps et al. 2014]. Additionally, the presence of distinctive cooling joints will enable such environmental settings to be readily recognised. However, the cut off of where these features stop forming has not been constrained. One account suggested that heavy rain during lava emplacement led to a thicker glassy rind [Macdonald 1953], and another noted thick glassy rinds on pāhoehoe flows that interacted with snow [Edwards et al. 2015]. The thickness of rind has also been shown to be influenced by non-hydrous cooling-enhanced environments, such as those that are windy [Keszthelyi and Denlinger 1996; Keszthelyi et al. 2003]. The thermal responsiveness of the outermost rind of a pāhoehoe lobe suggests that environmental conditions such as very low air temperatures, in addition to the presence or absence of water or wind, can influence glass content. However, the extent and conditions of this sort of cooling is not known. Cooling occurs in numerous stages from magma chamber to final equilibrium with the emplacement environment [Reeder et al. 2024]. For example, small crystals may grow in the conduit during ascent or in the lava during flow at the surface. Thus, it is important to assess the quality of the glass microscopically when using crystallinity and glassiness as a proxy for cooling rate. We investigate two aspects of glassiness, both the rind thickness and the crystal content of the outermost 50 µm of the rind, to examine the different effects emplacement environment might have on the sample overall.

Further, additional factors such as melt viscosity and mechanical erosion during and after emplacement can influence the rind formation and preservation. Erosion rates on young lava flows in dry locations with no visible erosion have been assumed to be 0—1 mm kyr^{-1} in geochronological studies, so pristine surfaces were presumed to have rind thickness that were close to original [Fenton and Niedermann 2014; Marchetti et al. 2014; Heineke et al. 2016]. Crystal kinetics and the glass forming ability of a lava must also be considered, since undercooling and degassing may increase polymerization in higher-silica melts (>57 wt.% SiO_2), causing suppressed nucleation and thus fewer crystals at slower cooling rates [Iezzi et al. 2008; Vetere et al. 2015]. To control for this, studies examining glass content of lava flows should consider the chemical composition of the lava as well as any stagnation or ponding that may have occurred on the flow field, which could promote further crystallization during emplacement.

Previous studies on Holocene basaltic lava flow rinds indicate that glass distribution across the surface of pāhoehoe flows can range from 20—100 %, which is partly due to variable thermal microenvironments [Rader et al. 2022; Reeder et al. 2024]. For example, vent material can either be very glassy from rapid quenching during ejection or have very little glass due to oxide crystal growth resulting from prolonged exposure to high-temperature gases [Rader et al. 2022]. Additionally, lava samples collected from the flow surface in the middle of a flow field (mid-flow) are generally glassier than samples collected from the outermost flow margins, although a good mechanism for this has not yet been identified [Reeder et al. 2024]. Thus, sampling a broad range of locations is important for capturing these environmental variations when attempting to characterize the overall cooling environment a lava flow experienced. Lava flows in the Rader et al. [2022] and Reeder et al. [2024] studies are located in the inland northwest USA between 41° and 43° (mid-) latitude at 1300—1700 meters elevation, erupted into a similar dry cold desert, and are similar bulk compositions (i.e. basalt). Thus, they provide a distinct group to compare with flows emplaced in colder environments to assess the effect that latitude and, thereby, climate, has on emplacement conditions. They are referred to as desert mid-latitude comparison flows. Further exploration into the variability of glass abundance across lava flow fields requires a wider range of emplacement environments than what is captured in these two previous studies.

1.3 Lost Jim lava flow and Camille lava flow

The two youngest flows in the Imuruk Lake volcanic field are both basaltic flows that were generated in an extensional tectonic setting and have not produced confident geochronological ages previously. The Lost Jim lava flow (65.4876, −163.2969) is a basaltic lava thought to be younger than the last glacial maximum [Hopkins 1963], although absolute dating has proven difficult. The lava was too young to be resolved by $^{40}Ar/^{39}Ar$ dating [Mukasa et al. 2007], whereas a ^{13}C date of 1655 ybp (years before present) of organic material from beneath an ash layer of unknown provenance near the flow field has confounding uncertainties [Kaufman and Hopkins 1985; Hopkins 1988]. Further uncertainty surrounds the impact the subarctic emplacement environment had on the morphology of the flow field with “collapse” pits that had been attributed to subsurface melting of permafrost by the lava flow [Begét and Kargel 2008; Marcucci et al. 2017]. However, a recent analysis of the flow morphology suggests that permafrost collapse was wrongly implicated as the cause of the pits across the surface of the flow [Orr et al. 2025]. Nevertheless, the subarctic emplacement environment of the Lost Jim flow field may have been substantially colder than the mid-latitude desert flows. Additionally, abundant surface water is found in lakes, streams, and perched on the tundra during the short summer, whereas ice and snow cover the region during the winter, all of which would increase cooling rates on lava flow surfaces [Hopkins 1959; Patrick et al. 2004; Edwards et al. 2014; 2015]. There are no classic indicators of lava-water interaction such

 9(2): 539–551. https://doi.org/10.30909/vol/hvex3566

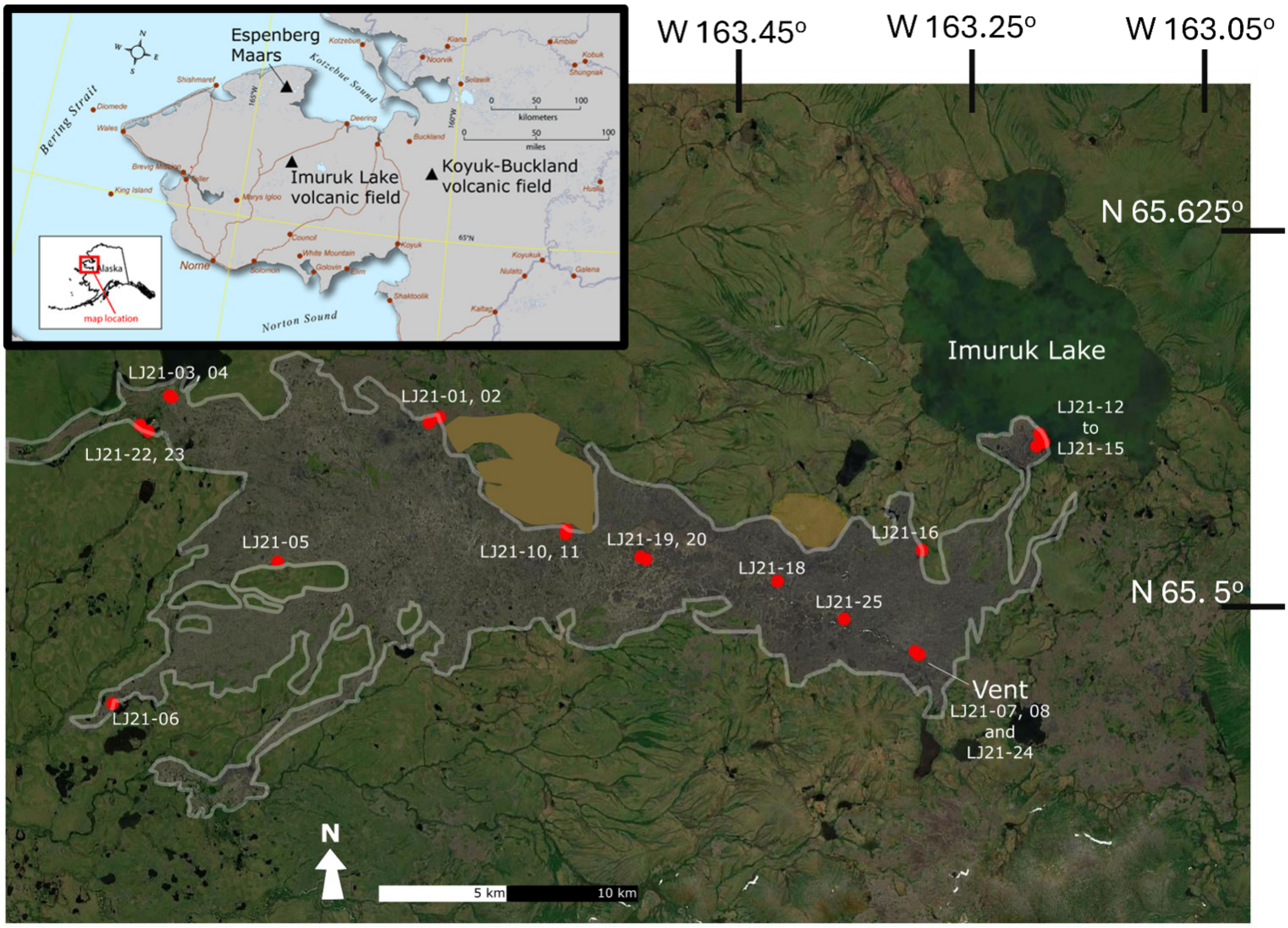

Figure 1: Location map with Lost Jim flow outlined in grey and Camille flow shaded in brown. Sample locations are shown as red dots with some dots overlapping. Zoomed in maps of these sampling localities can be found in Supplementary Material 1. Flow is located beneath the word 'Imuruk' in the zoomed out location map reproduced courtesy Schaefer, J. R. G. and the Alaska Volcano Observatory/Alaska Division of Geological & Geophysical Surveys. Satellite imagery is from Airbus and Maxar Technologies.

as hackly jointing, palagonite formation, pillow structures, or explosive deposits at Lost Jim flow field, indicating that water was not a dominant cooling mechanism. However, it is relevant to note the degree to which moisture is present, as this differs significantly from the desert comparison group. Surface morphology is dominated by inflated pāhoehoe with transitional morphologies lining only a few narrow channels, suggesting most of the lava was insulated from the environment until shortly before emplacement; thus the environment in the location of final emplacement is more likely to have influenced the cooling rate than changes during transport. To confirm the likelihood of a subarctic environment during emplacement given that climate has changed over time, we used ^{36}Cl to provide exposure dates for the flow.

The second youngest flow, the Camille flow, was also sampled in the hopes that it could provide additional glass data; however, the surface was so disrupted from frost wedging that determining primary surfaces was challenging and too few samples were collected to be utilized for the glass study. We do, however, report the ^{36}Cl dates for the underlying Camille flow to evaluate the timescales responsible for the extensive frost wedging across the flow. We surveyed the glass content of the rinds across a wide variety of lava surfaces at Lost Jim flow field to evaluate the potential impact that environmental factors may have had on the cooling history of the lava flow.

2 Methods and materials

2.1 Field

Helicopter-supported field work allowed for the collection of 23 lava and spatter samples across the flow field for petrographic analysis (Figure 1). The lava samples were predominantly from intact pāhoehoe surfaces, but two samples (LJ21-19 and 20) were from rubbly parts of the flow. Sites were selected for their emplacement environment based on previous study results that indicate microenvironments (e.g. wet margin, vent, mid-flow) may influence cooling rate, and samples were chosen to have intact, fresh surface textures exhibiting minimal erosion or weathering (Figure 2 and Table 1). Vent samples included intact and broken spatter surfaces, which were only selected if they had a coherent rind that resembled a flow surface and were not oxidized. Mid-flow samples were

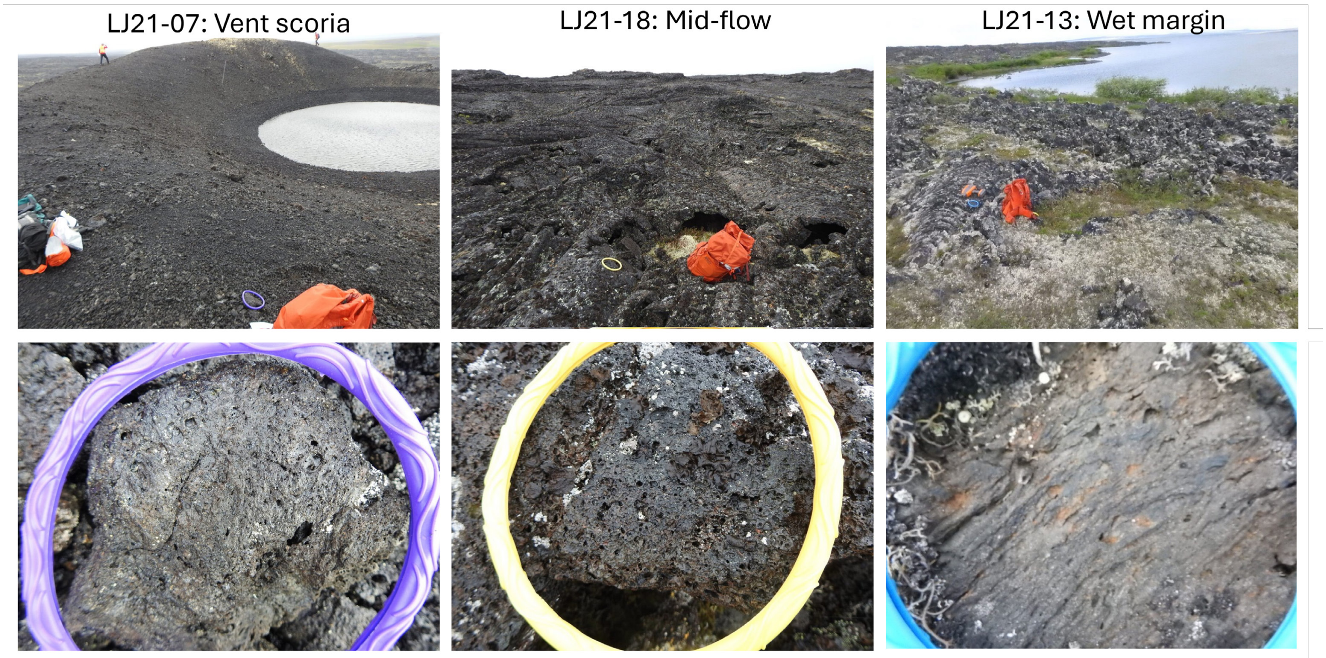

Figure 2: Example photo of vent, mid-flow, and wet margin. Sample rings are 15 cm in diameter. Images of all sampling sites can be found in Supplementary Material 1.

lava surfaces that were at least 20 m away from the farthest marginal extent of the flow. Margin samples were collected within 5 m along the farthest extent of the flow, with 'dry' samples showing no evidence of current water influence. Samples collected from 'wet margins' means substantial water existed at the margins at the time of sampling, not necessarily that water was present at the time of eruption [Rader et al. 2022; Reeder et al. 2024]. As lava flows can impound surface water after cooling, it is possible that modern-day 'wet' margins may not have been in direct contact with water at the time of eruption. However, as the chances of water being present at the time of emplacement is greater in these locations than in the 'dry' locations, there may have been a different influence on the cooling history or weathering history of the glass; thus, the current presence of water is noted for each sample. The only hornito sampled was a small rootless spatter pile located over a lava tube and unrelated to lava-water interactions. An additional eight samples from Lost Jim and Camille lava flows were collected for cosmogenic dating; we required thin and flat samples with an intact surface, with little shadowing from surrounding micro- and macro-topography.

2.2 ^{36}Cl exposure geochronology

^{36}Cl exposure dating is a method that has been successfully used to date young basaltic rocks [e.g. Zreda et al. 1993; Parmelee et al. 2015; Vazquez and Woolford 2015; Downs et al. 2021]. *In-situ* ^{36}Cl dating is based on the production of ^{36}Cl near the surface of the Earth due to the interaction of cosmogenic particles with Ca, K, Ti, Fe, and Cl in rocks. Calibrated production rates of ^{36}Cl can then be used to calculate the surface exposure age of a sample using the measured concentrations of ^{36}Cl and the sample geochemistry. The eight samples we collected for this purpose were surface slabs 6—9 cm thick and whole samples were processed instead of isolated mineral separates due to the fine-grained nature of the materials. Samples were sent to the Purdue University Rare Isotope Measurement (PRIME) Laboratory, Indiana, USA, for dissolution and measurement of ^{36}Cl. Dissolved whole rock separates were spiked with ^{35}Cl and concentrated. Cl isotopes were then measured using accelerator mass spectrometry. We calculated ages of the flows from ^{36}Cl concentration and sample geochemistry using the `CRONUScalc` v2.1 web interface [Marrero et al. 2016b; 2021]. We used the cosmogenic production rates of Lal [1991] and [Stone 2000] by selecting the 'Lm' scaling framework within `CRONUScalc`, which accounts for time variability in the strength of the magnetic field [Marrero et al. 2016a]. We assumed post-eruption erosion of the samples to be negligible based on the observation of the apparent youthfulness of volcanic surface features (e.g. fresh glassy surfaces, minimal lichen growth, and poor soil development on the surface). There also was no correlation between lava flow age and rim thickness, suggesting erosion was not a dominant process (Supplementary Material 1). Topographic shielding was also assumed to be negligible as samples were taken from prominent horizontal surfaces and the local topography is relatively flat [see Orr et al. 2025, for more discussion of flow morphology]. We used a bulk density of 2.8 g cm^{-3} and an attenuation length of 160 g cm^{2}. Whole rock major oxide and trace element data used in the calculations were acquired from Washington State University's (WSU) Peter Hooper GeoAnalytical Laboratory as part of a forthcoming companion study. Procedures for X-ray fluorescence analyses (XRF; major oxide data) and inductively coupled plasma mass spectrometry methods (ICP-MS; trace element data) are available from Knaack et al. [1994] and Johnson et al. [1999], respectively. An-

Table 1: Sample list for Lost Jim Lava Flow. * denotes a cosmogenic sample was collected in this vicinicty as well.

Sample name	Type	Latitude (°)	Longitude (°)	Glass rind thickness (mm)	Modal glass (%)
LJ21-01A	dry margin	65.568523	-163.709035	0.2	70
LJ21-01B	dry margin	65.568523	-163.709035	5.7	66
LJ21-02	dry margin	65.570467	-163.700111	11.0	71
LJ21-03	dry margin	65.577466	-163.925100	10.0	74
LJ21-04	dry margin	65.577995	-163.926848	15.4	79
LJ21-05	dry margin	65.520019	-163.835823	3.2	75
LJ21-06*	wet margin	65.470546	-163.974745	6.8	71
LJ21-07	vent scoria	65.487795	-163.297368	12.2	88
LJ21-08*	vent scoria	65.487737	-163.296325	0.2	77
LJ21-10	dry margin	65.531267	-163.592974	4.3	72
LJ21-11*	mid-flow	65.529791	-163.593594	1.1	60
LJ21-12	wet margin	65.564750	-163.195407	8.0	69
LJ21-13	wet margin	65.563433	-163.194209	7.0	76
LJ21-14	wet margin	65.561693	-163.191689	9.7	71
LJ21-15*	dry margin	65.560290	-163.198198	11.1	74
LJ21-16	dry margin	65.524309	-163.294249	8.3	69
LJ21-18*	mid-flow	65.513387	-163.415716	1.9	92
LJ21-19	mid-flow	65.521906	-163.531146	7.0	64
LJ21-20	mid-flow	65.521034	-163.526084	1.3	69
LJ21-22	wet margin	65.567833	-163.951387	0.2	67
LJ21-23	wet margin	65.565650	-163.944919	7.2	77
LJ21-24	mid-flow	65.488852	-163.300395	6.0	80
LJ21-25	hornito	65.500160	-163.359970	10.2	95
Average				6.4	74
Standard deviation				4.3	8

alytical precision for whole rock major and trace element data collected via the WSU GeoAnalytical Laboratory is discussed in Nye et al. [2018]. The full input table used to make the calculations can be found in Supplementary Material 1 Table S1.

2.3 Petrographic analysis

Hand samples were cut perpendicular to the surface to capture the change in texture from rind to interior and made into thin sections (Figure 3). In addition to examining the thickness of the rind, the number of crystals preserved in the outermost rind (~50 µm) was also measured. Eight to ten backscattered electron images were collected of the rind portion of the thin section with the Tescan VEGA-3 scanning electron microscope (SEM) housed at the U.S. Geological Survey Menlo Park (now Moffett Field), California, USA. Instrument conditions were set uniformly for all images collected. The accelerating voltage and working distance were set to 20 kV and 13 mm, respectively. Brightness and contrast were manually adjusted to optimally capture the observed textures. Magnification was set at 200× (FOV = 3.2 mm) for most images and increased to 600× (FOV = 1.08 mm) when necessary to observe fine textures.

Crystal modal percentage was calculated for each image using the program `ImageJ` [Schneider et al. 2012] to count the number of pixels (a proxy for crystal content) of each phase for glass, olivine, plagioclase, iron oxides, and vesicles [Rader et al. 2022; Reeder et al. 2024]. The starting crystal content was used to control for crystal growth during transport or stagnation. For samples with >9 % vesicles, the total glass value as reported in Tables 1 and 2 was calculated as the percent of the total minus the vesicle area. Thickness of glass rinds was also measured from thin sections magnified by 10× from the edge of the sample to the depth where the groundmass color turned from dark brown to black/opaque in plane polarized light as crystals become too thick to allow light to pass. The boundary between opaque and dark brown glass was distinct in all samples with rinds greater than 1 mm in thickness.

2.4 Comparative mid-latitude desert site selection

We compiled the modal percent of glass and rind thickness data from 31 previously published lava samples from volcanic fields in Oregon and Idaho, USA (Table 2). These include samples from Jordan Craters, analyzed by Reeder et al. [2024], and samples from Blue Dragon Flow, Diamond Craters, The Devil's Garden, Four Craters Lava Field, and Hells Half Acre, analyzed by Rader et al. [2022]. Geochemically, all samples are basalt or trachy-basalt with SiO_2 values ranging from 47—52 wt.% and total alkali values between 3.09 and 5.75 wt.%. The full geochemical analyses can be found in their respective publications and in Supplementary Material 1 Table S2. These samples all come from lava flows erupted in Cold Semi-Arid or Cold Desert regions, or BSk/BWk in the Köppen-Geiger climate classification [Beck et al. 2018]. Mean annual tempera-

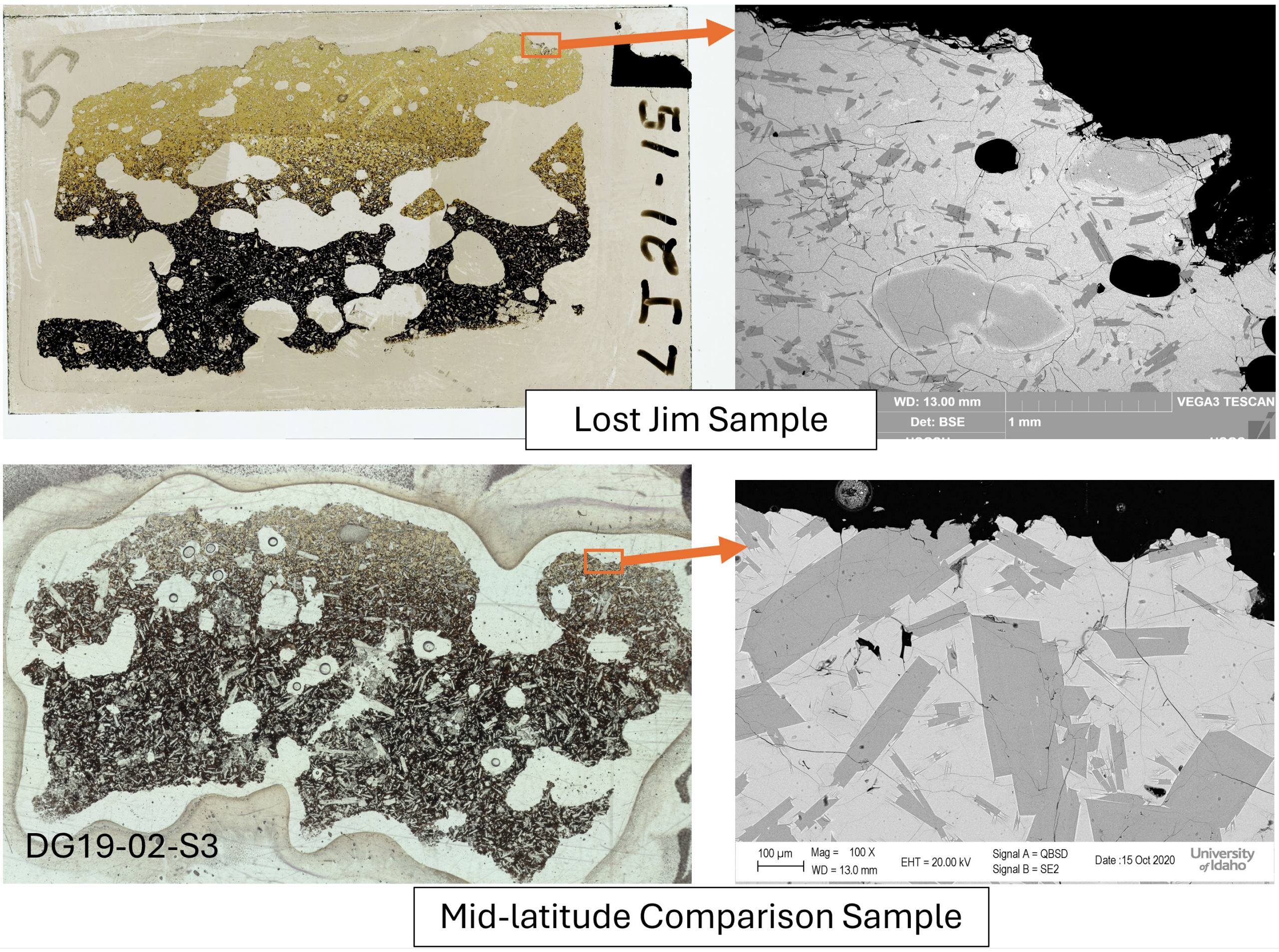

Figure 3: Thin section images showing rind thickness and scanning electron microscope (SEM) glass content. Top is Lost Jim flow, bottom is a mid-latitude comparison sample (Devils Garden, Oregon, USA). Images of all Lost Jim thin sections, SEM micrographs, and field photos can be found in the Supplementary Material 1.

tures of these sites are 5—10 °C, with mean winter minimum and summer maximum temperatures ranges of 5 to 0 °C and 20 to 28 °C, respectively [Arguez et al. 2010]. When compared to the Imuruk Lake volcanic field's Köppen-Geiger subarctic classification (Dfc), where the coldest month averages below 0 °C but at least three months have an average above 10 °C, the lavas from Oregon and Idaho were more likely to experience warmer temperatures and less precipitation/surface water. Bulk compositions of samples in this study are plotted against glass characteristics in Supplementary Material 1 and indicate the variability in the samples in this manuscript do not correlate with any aspect of geochemistry.

3 Results

3.1 ^{36}Cl ages and timescale of eruption

Calculated ages for the Lost Jim flow ranges from 6.80 ± 1.37 ka to 8.85 ± 2.1 ka, while the Camille flow ranged from 37.52 ± 6.97 ka to 43.56 ± 8.23 ka (1σ uncertainties including both analytical and production rate uncertainties, Table 3). This results in weighted mean ages of 7.73 ± 0.37 ka and 39.7 ± 1.3 ka, respectively, for those two flows (1σ including the analytical uncertainties only).

The duration of the Lost Jim eruption can be crudely estimated using its volume. Hopkins [1963] proposed a total volume of 3.3—4.2 km^3, which is 2—3 times the size of the 2014–2015 eruption of Holuhraun (1.44 km^3) in Iceland. The Holuhraun eruption was emplaced in about 6 months; however, the surface morphologies (tube-fed inflated pāhoehoe) at the Lost Jim flow indicate lower effusion rates than those at Holuhraun [channelized transitional morphologies; Voigt et al. 2021]. This suggests that the Lost Jim flow erupted on a timescale of years, and cooling rates were thus likely influenced by temperature variations over several seasonal cycles. As an unknown portion of the Camille flow is buried, no assessment was made of the duration or seasonality of this flow.

3.2 Glass content of rinds

The surface of the Camille flow was too degraded to ensure a robust sample of the original surface and so the thickness of the rind from the Camille samples are not included in this dataset. Although it is worth noting that, despite the high degree of erosion on the surface of the Camille flow, two of the

Table 2: Mid-latitude locations from Rader et al. [2022] and Reeder et al. [2024].

Sample name	Type	Glass rind thickness (mm)	Modal glass (%)
18-CPC-1	vent scoria	0.6	72
18-CPC-2A	vent spatter	0.3	72
18-CPC-2B	vent spatter	0.9	72
18-CPC-3	vent spatter	0.2	57
18-CPC-4	vent scoria	0.4	58
18-CPC-5	mid-flow	5.3	70
18-CPC-6	mid-flow	9.0	74
18-CPC-7B	wet margin	0.3	72
18-CPC-8	dry margin	0.2	56
18-CPC-9	dry margin	0.2	73
18-CPC-11	mid-flow	8.4	82
18-CPC-12	dry margin	6.8	62
18-CPC-13	vent spatter	0.2	46
BD19-7-S1	vent spatter	0.2	25
BD19-12-S2	hornito	0.2	78
BD19-19-S1	dry margin	6.4	69
BD19-20-S3	dry margin	0.2	82
DC19-4-S3	vent spatter	0.2	38
DC19-5-S3	vent spatter	3.0	71
DC19-10-S3	dry margin	2.5	71
DC19-11-s3	dry margin	0.2	34
DC19-13-S2	mid-flow	5.8	74
DG19-2-S3	dry margin	4.2	56
DG19-6-S2	vent scoria	9.3	68
DG19-9-S2	vent spatter	0.3	67
DG19-10-S2	dry margin	5.8	58
FC19-5-S3	vent scoria	5.5	60
FC19-6-S1	dry margin	0.2	24
HHA19-4-S2	vent spatter	0.2	27
HHA19-4-S3	vent spatter	0.2	39
HHA19-6-S2	vent spatter	0.2	76
Average		2.9	60
Standard deviation		3.1	17

Table 3: ^{36}Cl ages for the Lost Jim (white) and Camille (grey) flow samples.

Sample	Latitude (°)	Longitude (°)	Elevation (m)	Sample thickness (cm)	Bulk density (g cm^{-3})	Shielding factor	Erosion rate (mm yr^{-1})	Concentration ^{36}Cl (atoms/g)	^{36}Cl exposure date (ka)	Internal error (ka)	External error (ka)
21JFLLJ008	65.512442	-163.426029	368	8	2.8	1.000	0.00	73663	8.29	1.45	1.96
21LJTO-009	65.52892	-163.59077	251	8	2.8	1.000	0.00	101751	8.85	1.09	2.01
21LJTO-012	65.48738	-163.29563	458	6	2.8	1.000	0.00	89561	6.8	0.6	1.37
21LJTO-013	65.55865	-163.20453	325	9	2.8	1.000	0.00	100652	8.18	0.64	1.69
21LJTO-016	65.49052	-163.73143	183	7	2.8	1.000	0.00	92198	8.03	1.05	1.89
21LJTO-015	65.52621	-163.47423	325	8	2.8	1.000	0.00	483016	38.9	2.58	8.31
21LJTO-010	65.53192	-163.59082	253	6	2.8	1.000	0.00	419812	43.56	2.36	8.23
21LJTO-011	65.54716	-164.07938	92	11	2.8	1.000	0.00	296838	37.52	2.02	6.97

three collected samples still preserved some glassy rind, indicating the rind must have been thicker than the amount of erosion which as occurred. The modal percent of glass for the 23 Lost Jim flow field samples ranged from 60—95 % with an average of 74 ± 8 % (Table 1). No systematic difference in crystallinity percentage was noticed that might indicate vast differences in starting crystal content upon emplacement. Of the vesicle-free area, the remainder of the percentage was crystals of plagioclase, which were usually 2—4 times more abundant than olivine. No samples contained measurable oxides and only the three samples nearest the vent (LJ21-07, 08, and 24) contained large numbers of vesicles that required correction as described in the methods (Section 2.3). The average thickness of the rind of all the samples was 6.4 ± 4.3 mm with a range from 0.2 to 15.4 mm and a median value of 7 mm (Figure 4). Pyroclastic morphologies contained the most modal percentage of glass (vent scoria 82 % and hornito spatter 95 %), whereas margins and mid-flow samples all contained very similar amounts of glass (averages between 72 % and 74 %; Table 4 and Figure 5). Samples from dry margins had the highest average rind thickness (7.2 mm), followed by those from wet margins (6.5 mm), vent scoria (6.2 mm), and mid-flow samples (4.7 mm). The hornito sample had a glass rind of 4.3 mm.

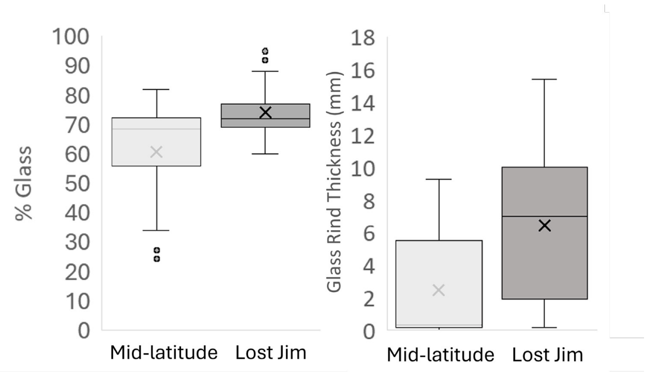

Figure 4: Two measures of glassiness from thin sections of the mid-latitude comparison group (light grey) and the Lost Jim flow (dark grey) samples. Plots are box and whisker plots which indicate the average by an 'X' and the median by a line in the middle of the box. Data for these plots are found in Table 1 and 2.

The modal percent of glass for the 31 desert samples ranged from 24 % to 82 % with an average of 60 ± 17 % (Table 2). The average rind thickness was 2.9 ± 3.1 mm, with a range from 0.2 to 9.3 mm and a median value of 0.3 mm (Figure 4). In these mid-latitude comparison samples, the highest modal percent glass content (78 %) was found in a single hornito sample, and the lowest (53 %) was found in vent spatter samples (Table 3 and Figure 5). Mid-flow samples, at 74 %, were similar to the single wet margin sample (72 %) but higher than the dry margin samples (58 %). Rind thickness was highest in the mid-flow samples at 7.1 mm, followed by scoria (4.0 mm) and dry margins (2.7 mm). The wet margin sample has a rind thickness of 0.3 mm.

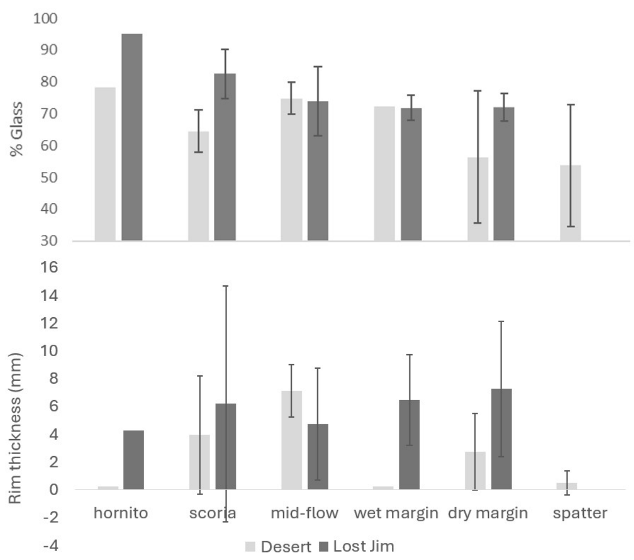

Figure 5: Two measures of glassiness (% glass: top; rind thickness: bottom) arranged by emplacement location. Mid-latitude samples are indicated in light grey and Lost Jim in dark grey. The error bars are 1σ. Data (averages for each group) for these graphs are found in Table 4.

4 Discussion

4.1 Lava flow field ages

Our ^{36}Cl age for the Lost Jim flow field of 7.73 ± 0.37 ka is significantly older than the previously hypothesized minimum age of 1655 ± 220 years [Kaufman and Hopkins 1985] but significantly younger than the age of the Camille flow at 39.7 ± 1.3 ka. The age for the Camille flow confirms the hypothesis that it erupted during a period of glaciation but is older than was thought previously [Middle as opposed to Late Wisconsin; Hopkins 1963]. Further, the surface erosion of the Camille flow provides a potential age constraint on the preservation potential of glassy rinds (e.g. flows in the 10s of thousands of years old should not be expected to retain original rinds). However, the cause for the erosion may have been the transition from glaciated period to non-glaciated as opposed to age and, hence, rinds may be present if extensive frost wedging in an older flow is not observed.

The previous age for the Lost Jim flow field comes from ^{13}C dates of organic material extracted from beneath an ash layer of unknown provenance on the north side of Imuruk Lake [Kaufman and Hopkins 1985]. The authors hypothesized that the ash came from the Lost Jim eruption; however, an explosive plume that produces ash-sized particles but no other explosive features, such as a caldera [Dzurisin et al. 1995; Freundt and Schmincke 1995], is uncommon for effusive basaltic eruptions and inconsistent with the products that might be expected from the explosive eruption of low-viscosity basalt, such as Pele's hair and tears produced by fountaining. Further, the distribution of the ash does not match a pattern expected from an eruption at the Lost Jim vent (e.g. none near the Lost Jim vent and too thin at the location sampled).

Table 4: Summary table.

		hornito	scoria	mid-flow	wet margin	dry margin	spatter
Modal glass (%)	Lost Jim	95	83	74	72	72	-
	Mid-latitude	78	64	75	72	56	54
	LJ std	-	8	11	4	4	-
	ML std	-	7	5	-	21	19
Rim thickness (mm)	Lost Jim	4.3	6.2	4.7	6.5	7.3	-
	Mid-latitude	0.2	4.0	7.1	0.3	2.7	0.5
	LJ std	-	8.5	4.0	3.3	4.9	-
	ML std	-	4.2	1.9	-	2.7	0.9

Abbreviations: Lost Jim = LJ, Mid-latitude = ML, and standard deviation = std.

One environmental variable that can impact the ^{36}Cl date is persistent snow cover, which can attenuate cosmogenic particles and reduce the cosmogenic production rate of ^{36}Cl. We did not account for this effect as it is difficult to estimate snow cover over geologic time. However, the nearest SNOTEL monitoring station (Pargon Creek, ~60 km south of Imuruk Lake) indicates that for the past 24 years between the months of November and May there is usually between 22—26 cm of snow [National Water and Climate Center 1999]. A study on ^{36}Cl ages at Mt. Erebus calculated that this amount of snow would impact the ages less than the analytical error of the measurement itself [Parmelee et al. 2015].

4.2 Climate during Lost Jim eruption

Given the ^{36}Cl ages, we must consider the climate during 6000—10,000 ybp, which is after the end of the last glacial maximum. During that time, the Imuruk Basin was ice-free but was very cold and windy [Hopkins 1963]. Modern-day weather conditions are an acceptable proxy, as average temperatures were within half a degree of modern values for the region between 6000 and 10,000 ybp [Colinvaux 1962; Herzschuh et al. 2023]. The mean annual temperature in Kotzebue, Alaska, the site of the weather station closest to the Lost Jim flow, was −5 °C over the period from 1981–2010, which is the extent of that dataset. As Kotzebue is coastal and Imuruk Lake is interior as well as 310 m higher in elevation, this temperature is likely warmer than that experienced by the eruption. A mean of −5 °C compares to a mean annual temperature of 5—10 °C for our comparison group of mid-latitude flows [Arguez et al. 2010]. Mean summer maximum and winter minimum temperatures are 15 °C and −8 °C for Kotzebue, respectively, and range from 20 to 28 °C and −5 to 0 °C for the mid-latitude sites. Given the volume estimate and the timescale of the Lost Jim eruption, the flowing lava experienced both the cold, windy conditions during the 7—8 months of winter as well as the swampy, thaw lake-covered tundra during the brief cool summer [Hopkins 1959]. Thus, it is reasonable to assume the cooling environment during emplacement of most of the Lost Jim flow included a combination of cold, snowy, icy, wet, and windy conditions.

4.3 Glass distribution on the lava surface

The quenched rinds from all samples from the top of the Lost Jim flow field tend to have, on average, 14 % more glass than the mid-latitude flows measured for this study. Additionally, the least glassy sample from the Lost Jim flow field was the same percentage as the average of the desert comparison group (60 %). A t-test indicated that all the samples in the two groups are significantly different with p values < 0.001. It is possible that samples with less glassy rinds could be found at the Lost Jim flow field if targeted sampling was conducted; however, methods for sample collection were the same between all field sites, suggesting that the difference between the different latitudes is not due to sampling bias. The thickness of the glassy rinds from the Lost Jim flow extends, on average, twice as deep as the comparison group, indicating that the crust of the Lost Jim flow cooled faster than typical cold desert air-cooled lava flows. Rind thickness (Figure 4) varies more in the Lost Jim flow field samples, showing that, even in subarctic conditions, a very thin glassy rind may form, as some samples may be erupted during a warm portion of a day with no wind during the summer or protected from the harsh weather by microtopography.

The modal percent glass content of the Lost Jim flow samples was highest for unoxidized pyroclastics, which is similar for our comparison group. However, unlike the desert lava samples, the difference in glass content at the margins and the middle of the Lost Jim flow did not vary greatly, indicating that the main control on cooling was likely the cold air temperature rather than environmental conditions that would have a bigger impact on the margins (e.g. shallowly ponded water). This also suggests that while a universal mechanism for the difference in margin and mid-flow glass contents for the comparison group is not known, the differences in cooling environment between these locations in the comparison group were greater.

Glassy rind thickness for the Lost Jim samples also tended to be greater than the mid-latitude samples in all the emplacement locations except mid-flow (Figure 5). In general, the samples with higher glass contents had thicker visible glassy rinds; however, there is a lot of variability within the samples, indicating that slight differences in the cooling environment may be influencing these two measures of glass content (rind thickness and modal percent of glass). Our data set does not contain enough samples to do further statistics on what other aspects of the samples might be correlating with the variability. Our findings suggest that glass distribution in intact, unaltered lava flow surfaces records cooling histories that reflect the emplacement environment. Flow fields that have a continuous glass content of ~70 % along their margins may have experienced enhanced cooling from a colder environmental temperature or persistent wind, whereas discontinuous glassy margins may indicate brief or local surface water interaction during emplacement.

4.4 Glassiness as an indicator for emplacement environment

The thickness of the glassy rind on the surface of a lava flow, as well as the rind's modal percentage of glass, may reflect environmental conditions that produce faster cooling rates. However, it is important to note that the impact of climate and seasonality can overlap with shorter-duration flows. Our dataset compares the Lost Jim flow field to six other lava flows; all erupted in unknown weather conditions. Extreme weather (e.g. cold snaps, freezing rain, monsoons, blizzards) during an eruption may be the cause for some of the glassiness in the desert mid-latitude control group. An additional factor that could lead to thick glassy rinds in mafic lavas regardless of environmental conditions includes overpressurization or stagnation inside an inflated lobe, which allows for either resorption of vesicle gas or degassing and a subsequent densification of the glassy outer rind of the subsequent breakout [Sage 2000; Kauahikaua et al. 2003; Oze and Winter 2005]. Thus, if utilizing this method, it is important to consider the location of the sample you are collecting. For example, margin and mid-flow samples are more likely than vent samples to be influenced by environmental conditions while cooling. Likewise, a few samples may not be enough to indicate a broad cooling environment, since samples air-quenched in any climate can end up highly glassy. Instead, a wide variety of samples should be assessed, and outliers evaluated for microenvironmental impacts, such as emplacement in a sheltered or insulated area, a clastogenic origin, or emplacement near a heat source, like a fumarole. Additionally, glassy rinds that do not have vesicles should be treated with caution in paleoenvironmental studies, as these thick rinds are attributed to lava flow dynamics instead of the local environment. Further study could help to understand the relationship between glass rind thickness, petrographic textures, and microlite growth and to better interpret emplacement environments and to understand the sensitivity lava flows may have to climate-related cooling.

Lava rinds must be preserved sufficiently (i.e. not physically weathered, though altered is acceptable if rind thickness is still distinct as can be the case for palagonitization) for an accurate assessment of the cooling environment during emplacement; thus, this method may not be as widely applicable to basaltic environments as hoped. However, glassy rinds have been found to be preserved in lavas 10–100s of millions of years old, such as the Deccan Traps, Columbia River Flood Basalts, and the Paraná Flood Basalts [Duraiswami et al. 2001; Waichel et al. 2006; Bondre and Hart 2008]. Volcanically active locations that lack other paleoclimate records, such as small islands with no lakes, coral reefs, or glaciers, may benefit from this sort of climate information. This method, which requires no analytical capabilities beyond magnification, could be applied to other planetary surfaces with volcanic activity or impact, to constrain regional or temporal changes in climate without the need for isotopic analysis.

5 Conclusions

We provide the first geochronological dates for the Lost Jim flow, which erupted 7.73 ± 0.37 ka, and the Camille flow, which erupted 39.7 ± 1.3 ka. Despite emplacement of the Lost Jim flow being substantially after the last glacial maximum, the climate at that time was cold and windy, similar to today. The Lost Jim flow field, with an estimated volume of ~4 km^3, was probably emplaced on the timescale of years as opposed to months, necessitating some portion of the eruption occurring during the subarctic winter. The impact of the emplacement of the Lost Jim flow field during cold subarctic conditions may have influenced the formation of the glass content of the outermost rind of samples collected from across the flow field. The overall modal percentage of glass on a microscopic scale was greater than lava flows emplaced in the mid-latitude United States (74 % vs 60 %, respectively), with Lost Jim flow field samples extending to higher values. The thickness of the glass rind measured from standard 30 µm thick petrographic thin sections was also greater (6.4 mm to 2.9 mm). The pattern of glassiness at the Lost Jim flow field generally follows that seen at other flows, with hornito spatter and unoxidized vent scoria having the highest glass contents, and glass contents of mid-flow samples being higher than those of margin samples. However, Lost Jim flow field samples exhibited less variability between the mid-flow and margin environments, suggesting cooling rates may have been buffered by a widespread factor, such as colder average temperatures, as opposed to water along the margins of the flow. Even though the weather during emplacement for the comparison desert lava flows is unknown, and each desert location is capable of overlap in extreme temperatures, moisture content, and wind magnitude, the cumulative evaluation of the glassiness of those samples suggests slower cooling times for the outer rinds of the mid-latitude lava flows. This study illustrates how measures of glassiness of the surface rind on an unaltered and largely intact lava flow may form in response to subarctic temperatures during lava flow emplacement, providing an additional temperature proxy for volcanically active areas. Lava flows with thick glassy rinds in places with few climate records could indicate time periods with significantly colder temperatures. Conversely, thin glassy rinds across a flow field may indicate a warmer climate at the time of emplacement. This relationship may be particularly important for locations such as Mars, where sedimentary rock paleoclimate data are limited, but lava flows are abundant and widespread [Tanaka et al. 2014]. Lava rind thickness analysis could also help extend climate records on small volcanically active, terrestrial islands which lack other climate proxies such as lake sediment or ice core records. Further study to understand the broad application of this technique could be beneficial, as the impact of numerous other factors, such as flow thickness, was not compared between flows, and because the hypothesized environmental conditions at the time of emplacement were not measured. However, the differences in glassiness shown in this paper suggests that a wider study that includes flows from more climates and observations of small-scale emplacement environments with collected samples of modern eruptions may allow for a broader application of this finding.

Author Contributions

ER conceived of the project, obtained funding, conducted field work, analyzed the majority of the SEM and petrographic images, and wrote the majority of the first draft text and figures. JL and TO participated in field work and field discussions and provided whole rock geochemical data for the geochronology models. DR imaged the petrographic slides with the SEM and slide scanner for glass content analysis. JS interpreted the ^{36}Cl data and contributed to the first draft text. All authors edited the manuscript.

Acknowledgements

Funding for this project was provided by NASA PSTAR award 80NSSC18K1518. Field work coordination and support was provided by the Alaska Volcano Observatory. Samples were collected under the National Park Service permit BELA-2021-SCI-0003. Modal % calculations for ¼ of the SEM images were completed by Owen Carswell to fulfil a workstudy position. Any use of trade, firm, or product names is for descriptive purposes only and does not imply endorsement by the U.S. Government.

Data Availability

All data are published as appendices with this article.

Copyright Notice

References

Arguez, A., I. Durre, S. Applequist, M. Squires, R. Vose, X. Yin, and R. Bilotta (2010). *U.S. Climate Normals Product Suite (1981–2010)*. DOI: 10.7289/V5PN93JP.

Beck, H. E., N. E. Zimmermann, T. R. McVicar, N. Vergopolan, A. Berg, and E. F. Wood (2018). "Present and future Köppen-Geiger climate classification maps at 1-km resolution". *Scientific Data* 5(1). DOI: 10.1038/sdata.2018.214.

Begét, J. E. and J. S. Kargel (2008). "Volcanoes and permafrost in Bering Land Bridge National Preserve, arctic Alaska". *Alaska Park Science* 7(1), pages 33–37.

Bondre, N. R. and W. K. Hart (2008). "Morphological and textural diversity of the Steens Basalt lava flows, Southeastern Oregon, USA: implications for emplacement style and nature of eruptive episodes". *Bulletin of Volcanology* 70(8), pages 999–1019. DOI: 10.1007/s00445-007-0182-x.

Colinvaux, P. A. (1962). *The environment of the Bering land bridge*. Duke University.

Deschamps, A., C. Grigné, M. Le Saout, S. A. Soule, P. Allemand, B. Van Vliet-Lanoe, and F. Floc'h (2014). "Morphology and dynamics of inflated subaqueous basaltic lava flows". *Geochemistry, Geophysics, Geosystems* 15(6), pages 2128–2150. DOI: 10.1002/2014GC005274.

Downs, D. T., D. E. Champion, M. A. Clynne, and L. J. P. Muffler (2021). "A Multidisciplinary Investigation Into the Eruptive Style, Processes, and Duration of a Cascades Back-Arc Tholeiitic Basalt: A Case Study of the Brushy Butte Flow Field, Northern California, United States". *Frontiers in Earth Science* 9, page 639459. DOI: 10.3389/feart.2021.639459.

Duraiswami, R. A., N. R. Bondre, G. Dole, V. M. Phadnis, and V. S. Kale (2001). "Tumuli and associated features from the western Deccan Volcanic Province, India". *Bulletin of Volcanology* 63(7), pages 435–442. DOI: 10.1007/s004450100160.

Dzurisin, D., J. P. Lockwood, T. J. Casadevall, and M. Rubin (1995). "The Uwekahuna Ash Member of the Puna Basalt: product of violent phreatomagmatic eruptions at Kilauea volcano, Hawaii, between 2800 and 2100 ^{14}C years ago". *Journal of Volcanology and Geothermal Research* 66(1-4), pages 163–184. DOI: 10.1016/0377-0273(94)00062-l.

Edwards, B. R., A. Belousov, and M. Belousova (2014). "Propagation style controls lava–snow interactions". *Nature Communications* 5, page 5666. DOI: 10.1038/ncomms6666.

Edwards, B. R., A. Belousov, M. Belousova, and D. Melnikov (2015). "Observations on lava, snowpack and their interactions during the 2012–13 Tolbachik eruption, Klyuchevskoy Group, Kamchatka, Russia". *Journal of Volcanology and Geothermal Research* 307, pages 107–119. DOI: 10.1016/j.jvolgeores.2015.08.010.

Fenton, C. R. and S. Niedermann (2014). "Surface exposure dating of young basalts (1–200 ka) in the San Francisco volcanic field (Arizona, USA) using cosmogenic ^{3}He and ^{21}Ne". *Quaternary Geochronology* 19, pages 87–105. DOI: 10.1016/j.quageo.2012.10.003.

Freundt, A. and H.-U. Schmincke (1995). "Eruption and emplacement of a basaltic welded ignimbrite during caldera formation on Gran Canaria". *Bulletin of Volcanology* 56(8), pages 640–659. DOI: 10.1007/bf00301468.

Griffiths, R. W. (2000). "The Dynamics of Lava Flows". *Annual Review of Fluid Mechanics* 32(1), pages 477–518. DOI: 10.1146/annurev.fluid.32.1.477.

Harris, A. and S. K. Rowland (2001). "FLOWGO: a kinematic thermo-rheological model for lava flowing in a channel". *Bulletin of Volcanology* 63(1), pages 20–44. DOI: 10.1007/s004450000120.

Head, J. W. and L. Wilson (1986). "Volcanic processes and landforms on Venus: Theory, predictions, and observations". *Journal of Geophysical Research: Solid Earth* 91(B9), pages 9407–9446. DOI: 10.1029/jb091ib09p09407.

Heineke, C., S. Niedermann, R. Hetzel, and C. Akal (2016). "Surface exposure dating of Holocene basalt flows and cinder cones in the Kula volcanic field (Western Turkey) using cosmogenic 3He and 10Be". *Quaternary Geochronology* 34, pages 81–91. DOI: 10.1016/j.quageo.2016.04.004.

Herzschuh, U., T. Böhmer, M. Chevalier, R. Hébert, A. Dallmeyer, C. Li, X. Cao, O. Peyron, L. Nazarova, E. Y. Novenko, J. Park, N. A. Rudaya, F. Schlütz, L. S. Shumilovskikh, P. E. Tarasov, Y. Wang, R. Wen, Q. Xu, and Z. Zheng (2023). "Regional pollen-based Holocene temperature and precipitation patterns depart from the Northern Hemisphere mean trends". *Climate of the Past* 19(7), pages 1481–1506. DOI: 10.5194/cp-19-1481-2023.

Hirashima, K. B. (1952). "Rate of cooling of lava flows". *Proceedings of the Thirty-First Annual Meeting of the Highway Research Board, Washington, D.C.* Volume 31.

Hopkins, D. M. (1959). "History of Imuruk Lake, Seward Peninsula, Alaska". *Geological Society of America Bulletin* 70(8), pages 1033–1046. DOI: 10.1130/0016-7606(1959)70[1033:HOILSP]2.0.CO;2.

– (1963). *Geology of the Imuruk Lake area, Seward Peninsula, Alaska*. Report Bulletin 1141-C. U.S. Geological Survey. DOI: 10.3133/b1141c.

– (1988). *The Espenberg Maars; a Record of Explosive Volcanic Activity in the Devil Mountain-Cape Espenberg Area, Seward Peninsula, Alaska*. National Park Service, Alaska Regional Office.

Iezzi, G., S. Mollo, G. Ventura, A. Cavallo, and C. Romano (2008). "Experimental solidification of anhydrous latitic and trachytic melts at different cooling rates: The role of nucleation kinetics". *Chemical Geology* 253(3-4), pages 91–101. DOI: 10.1016/j.chemgeo.2008.04.008.

Johnson, D., P. Hooper, and R. Conrey (1999). "XRF method XRF analysis of rocks and minerals for major and trace elements on a single low dilution Li-tetraborate fused bead". *Advances in X-ray Analysis* 41, pages 843–867.

Kauahikaua, J., D. R. Sherrod, K. V. Cashman, C. Heliker, K. Hon, T. N. Mattox, and J. A. Johnson (2003). "Hawaiian lava-flow dynamics during the Puu Oo-Kupaianaha eruption: A tale of two decades". *The Pu'u 'Ō'ō-Kūpaianaha eruption of Kılauea Volcano, Hawai'i: The first 20 years*. Edited by C. C. Heliker, D. A. Swanson, and T. J. Takahashi. U.S. Geological Survey Professional Paper 1676. Reston, VA: U.S. Geological Survey, pages 63–88. DOI: 10.3133/pp1676.

Kaufman, D. S. and D. M. Hopkins (1985). *Late Cenozoic radiometric dates, Seward and Baldwin Peninsulas, and adjacent continental shelf, Alaska*. DOI: 10.3133/ofr85374.

Keszthelyi, L. and R. Denlinger (1996). "The initial cooling of pahoehoe flow lobes". *Bulletin of Volcanology* 58(1), pages 5–18. DOI: 10.1007/s004450050121.

Keszthelyi, L., A. J. L. Harris, and J. Dehn (2003). "Observations of the effect of wind on the cooling of active lava flows". *Geophysical Research Letters* 30(19). DOI: 10.1029/2003GL017994.

Knaack, C., S. Cornelius, and P. R. Hooper (1994). *Trace Element Analyses of Rocks and Minerals by ICP-MS*. Open File Report. Department of Geology, Washington State University.

Lal, D. (1991). "The present scope of the field of terrestrial cosmogenic nuclides". *Current Science*, pages 744–751.

Lescinsky, D. T. and J. H. Fink (2000). "Lava and ice interaction at stratovolcanoes: Use of characteristic features to determine past glacial extents and future volcanic hazards". *Journal of Geophysical Research: Solid Earth* 105(B10), pages 23711–23726. DOI: 10.1029/2000JB900214.

Macdonald, G. A. (1953). "Pahoehoe, aa, and block lava". *American Journal of Science* 251(3). DOI: 10.2475/ajs.251.3.169.

Marchetti, D. W., S. A. Hynek, and T. E. Cerling (2014). "Cosmogenic ^{3}He exposure ages of basalt flows in the northwestern Payún Matru volcanic field, Mendoza Province, Argentina". *Quaternary Geochronology* 19, pages 67–75. DOI: 10.1016/j.quageo.2012.10.004.

Marcucci, E. C., C. W. Hamilton, and R. R. Herrick (2017). "Remote sensing evidence of lava–ground ice interactions associated with the Lost Jim Lava Flow, Seward Peninsula, Alaska". *Bulletin of Volcanology* 79, page 89. DOI: 10.1007/s00445-017-1176-y.

Marrero, S. M., F. M. Phillips, B. Borchers, N. Lifton, R. Aumer, and G. Balco (2016a). "Cosmogenic nuclide systematics and the CRONUScalc program". *Quaternary Geochronology* 31, pages 160–187. DOI: 10.1016/j.quageo.2015.09.005.

Marrero, S. M., F. M. Phillips, M. Caffee, and J. Gosse (2021). "Corrigendum to "CRONUS-Earth cosmogenic ^{36}Cl calibration" [Quat. Geochronol. 31 (2016) 199–219]". *Quaternary Geochronology* 61, page 101130. DOI: 10.1016/j.quageo.2020.101130.

Marrero, S. M., F. M. Phillips, M. W. Caffee, and J. C. Gosse (2016b). "CRONUS-Earth cosmogenic ^{36}Cl calibration". *Quaternary Geochronology* 31, pages 199–219. DOI: 10.1016/j.quageo.2015.10.002.

Mee, K., H. Tuffen, and J. Gilbert (2006). "Snow-contact volcanic facies and their use in determining past eruptive environments at Nevados de Chillán volcano, Chile". *Bulletin of volcanology* 68(4), pages 363–376. DOI: 10.1007/s00445-005-0017-6.

Mukasa, S. B., A. V. Andronikov, and C. M. Hall (2007). "The ^{40}Ar/^{39}Ar chronology and eruption rates of Cenozoic volcanism in the eastern Bering Sea Volcanic Province, Alaska". *Journal of Geophysical Research: Solid Earth* 112(B6). DOI: 10.1029/2006JB004452.

National Water and Climate Center (1999). *Sourdough Gulch (986) SNOTEL Site*. Accessed: 2024-02-29, https://wcc.sc.egov.usda.gov/nwcc/site?sitenum=986.

Nichols, A., M. Potuzak, and D. Dingwell (2009). "Cooling rates of basaltic hyaloclastites and pillow lava glasses from the HSDP2 drill core". *Geochimica et Cosmochimica Acta* 73(4), pages 1052–1066. DOI: 10.1016/j.gca.2008.11.023.

Nye, C., J. Begét, P. Layer, M. Mangan, V. McConnell, R. McGimsey, T. Miller, R. Moore, and P. Stelling (2018). *Geochemistry of some quaternary lavas from the Aleutian Arc and Mt. Wrangell*. Technical report. DOI: 10.14509/29843.

Orr, T. R., W. M. Coombs, E. Rader, and J. Larsen (2025). "Does the Lost Jim lava flow (Alaska) really preserve evidence of interaction with permafrost?" *Journal of Volcanology and Geothermal Research* 464, page 108347. DOI: 10.1016/j.jvolgeores.2025.108347.

Oze, C. and J. D. Winter (2005). "The occurrence, vesiculation, and solidification of dense blue glassy pahoehoe". *Journal of Volcanology and Geothermal Research* 142(3-4), pages 285–301. DOI: 10.1016/j.jvolgeores.2004.11.008.

Parmelee, D. E., P. R. Kyle, M. D. Kurz, S. M. Marrero, and F. M. Phillips (2015). "A new Holocene eruptive history of Erebus volcano, Antarctica using cosmogenic ^{3}He and ^{36}Cl exposure ages". *Quaternary Geochronology* 30, pages 114–131. DOI: 10.1016/j.quageo.2015.09.001.

Patrick, M. R., J. Dehn, and K. Dean (2004). "Numerical modeling of lava flow cooling applied to the 1997 Okmok eruption: Approach and analysis". *Journal of Geophysical Research: Solid Earth* 109(B3). DOI: 10.1029/2003jb002537.

Rader, E., S. Ackiss, A. Sehlke, J. Bishop, B. Orrill, K. Odegaard, M. Meier, and A. Doloughan (2022). "Average VNIR reflectance: A rapid, sample-free method to estimate glass content and crystallinity of fresh basaltic lava". *Icarus* 383, page 115084. DOI: 10.1016/j.icarus.2022.115084.

Reeder, A., E. Rader, and J. Bishop (2024). "Glass, crystallinity, and VNIR reflectance from vent to margin at Jordan Craters, OR USA". *Journal of Volcanology and Geothermal Research* 447, page 108035. DOI: 10.1016/j.jvolgeores.2024.108035.

Rowland, S. K., A. J. L. Harris, and H. Garbeil (2004). "Effects of Martian conditions on numerically modeled, cooling-limited, channelized lava flows". *Journal of Geophysical Research: Planets* 109(E10). DOI: 10.1029/2004je002288.

Sage, L. L. (2000). "A Study of Dense, Glassy Flows: Dense Pahoehoe Lava Flows From Kilauea Volcano, Hawaii". *McNair Scholars Journal* 4(1), page 5.

Schneider, C. A., W. S. Rasband, and K. W. Eliceiri (2012). "NIH Image to ImageJ: 25 years of image analysis". *Nature Methods* 9(7), pages 671–675. DOI: 10.1038/nmeth.2089.

Stone, J. O. (2000). "Air pressure and cosmogenic isotope production". *Journal of Geophysical Research: Solid Earth* 105(B10), pages 23753–23759. DOI: 10.1029/2000JB900181.

Tanaka, K. L., J. A. Skinner, J. M. Dohm, R. P. Irwin, E. J. Kolb, C. M. Fortezzo, T. Platz, G. G. Michael, and T. M. Hare (2014). *Geologic map of Mars*. DOI: 10.3133/sim3292.

Vazquez, J. A. and J. M. Woolford (2015). "Late Pleistocene ages for the most recent volcanism and glacial-pluvial deposits at Big Pine volcanic field, California, USA, from cosmogenic ^{36}Cl dating". *Geochemistry, Geophysics, Geosystems* 16(9), pages 2812–2828. DOI: 10.1002/2015GC005889.

Vetere, F., G. Iezzi, H. Behrens, F. Holtz, G. Ventura, V. Misiti, A. Cavallo, S. Mollo, and M. Dietrich (2015). "Glass forming ability and crystallisation behaviour of sub-alkaline silicate melts". *Earth-Science Reviews* 150, pages 25–44. DOI: 10.1016/j.earscirev.2015.07.001.

Voigt, J. R. C., C. W. Hamilton, G. Steinbrügge, and S. P. Scheidt (2021). "Surface roughness characterization of the 2014–2015 Holuhraun lava flow-field in Iceland: implications for facies mapping and remote sensing". *Bulletin of Volcanology* 83(12). DOI: 10.1007/s00445-021-01499-4.

Waichel, B. L., E. F. de Lima, R. Lubachesky, and C. A. Sommer (2006). "Pahoehoe flows from the central Paraná Continental Flood Basalts". *Bulletin of Volcanology* 68(7-8), pages 599–610. DOI: 10.1007/s00445-005-0034-5.

Wilding, M., D. Dingwell, R. Batiza, and L. Wilson (2000). "Cooling rates of hyaloclastites: applications of relaxation geospeedometry to undersea volcanic deposits". *Bulletin of Volcanology* 61(8), pages 527–536. DOI: 10.1007/s004450050003.

Wilding, M., S. Webb, and D. Dingwell (1995). "Evaluation of a relaxation geospeedometer for volcanic glasses". *Chemical Geology* 125(3-4), pages 137–148. DOI: 10.1016/0009-2541(95)00067-V.

Wilding, M., S. Webb, D. Dingwell, G. Ablay, and J. Marti (1996). "Cooling rate variation in natural volcanic glasses from Tenerife, Canary Islands". *Contributions to mineralogy and petrology* 125(2), pages 151–160. DOI: 10.1007/s004100050212.

Zreda, M. G., F. M. Phillips, P. W. Kubik, P. Sharma, and D. Elmore (1993). "Cosmogenic ^{36}Cl dating of a young basaltic eruption complex, Lathrop Wells, Nevada". *Geology* 21(1), page 57. DOI: 10.1130/0091-7613(1993)021<0057:CCDOAY>2.3.CO;2.